

A numerical study of the nanoribbon field-effect transistors under the ballistic and dissipative transport

Seyed Saleh Ghoreishi¹ · Reza Yousefi¹ · Kamyar Saghafi² · Habib Aderang¹

Received: 23 January 2017 / Accepted: 9 August 2017 / Published online: 20 August 2017
© The Author(s) 2017. This article is an open access publication

Abstract In this article, a detailed performance comparison is made between ballistic and dissipative quantum transport of metal oxide semiconductor-like graphene nanoribbon field-effect transistor, in ON and OFF-state conditions. By the self-consistent mode-space non-equilibrium Green's function approach, inter- and intraband scattering is accounted and the role of acoustic and optical phonon scattering on the performance of the devices is evaluated. We found that in this structure the dominant mechanism of scattering changes according to the ranges of voltage bias. Under large biasing conditions, the influence of optical phonon scattering becomes important. Also, the ambipolar and OFF-current are impressed by the phonon-assisted band-to-band tunneling and increased considerably compared to the ballistic conditions, although sub-threshold swing degrades due to optical phonon scattering.

Keywords Optical phonon scattering (OP) · Acoustic phonon scattering (AP) · Born approximation · Graphene nanoribbon (GNR) · Band-to-band tunneling (BTBT)

Introduction

Owing to their excellent scalability properties, silicon devices have enjoyed high popularity in the past few decades. Today, by the shrinkage in the dimensions of different technologies and entry of nanoscale dimensions, these devices have encountered numerous physical constraints [1, 2] which have increasingly necessitated the need for new nano-electrical devices and new manufacturing technology. Meanwhile, graphene seems to be a good alternative and, in recent years, has attracted great attention. Non-defective graphene is a zero band-gap material as a sheet consisting of carbon atoms which are juxtaposed in a hexagonal structure [3–6]. The absence of a band-gap limits the performance of the transistors and degrades some characteristics of them like on/off ratio. To open the band-gap, graphene is patterned into carbon nanotubes (CNTs) and graphene nanoribbons (GNRs).

GNR is presently being explored as a workable option to use instead of Si as the channel material of field-effect transistors (FETs).

One type of graphene nanoribbon-based field-effect transistors (GNRFETs) is metal oxide semiconductor (MOS)-like GNRFET [7–10]. In the MOS-like GNRFET, applying a gate voltage can reduce the potential barrier at the channel region, leading to flowing of carriers from the top of the barrier and reaching the drain side. So that, the On-current is of thermionic type in this structure. Also, the off-current in this structure is of the band-to-band tunneling (BTBT) type. The purpose of this paper is to examine how phonon scattering affects the performance of MOS-like GNRFET.

Many works have been done for GNR (CNT)-FETs but most of them are in the ballistic limit [11–13]. Factors such as electron–phonon interaction can also affect the electrical

✉ Seyed Saleh Ghoreishi
salehghoreyshi@gmail.com; S.ghoreishi@iaunour.ac.ir

Reza Yousefi
r.yousefi@iaunour.ac.ir

Kamyar Saghafi
saghafi@shahed.ac.ir

Habib Aderang
habibadrang@gmail.com

¹ Department of Electrical Engineering, Nour Branch, Islamic Azad University, Nour, Iran

² Department of Electrical Engineering, Shahed University, P.O. Box 18155-159, Tehran 3319118651, Iran

properties of graphene ribbons [14, 15]. In practice, graphene-based field-effect transistors with a long channel demonstrate non-ballistic behaviors. Thus, in order to show the real behavior of a device, scattering effects and scattering mechanisms should be considered. So far, some studies have been done in this regard, most of which have been based on CNT [16–19]. Further, in previous reports, interband scattering effects have been neglected. Note that the energy difference between first and second sub-band increases as the GNR width increases. So that, a significant coupling between sub-bands by phonon is created which necessitates that interband scattering is regarded. In this article, we are going to investigate the effects of optical and acoustic phonon scattering on the performance of MOS-like graphene nanoribbon-based field-effect transistors and examine the extent and manner of the effects of these factors on each of the thermionic and tunneling currents. For the simulation, we used the non-equilibrium Green's function (NEGF) procedure, in which the effects of electron–phonon interaction enter Green's function as a self-scattering matrix. Furthermore, in the simulation procedure, both the intraband and interband phonon scattering effects were regarded in the software simulation.

In the rest of the paper, in “[Simulation method](#)”, we will describe the simulation method. In “[Simulation results and discussion](#)”, the results of the simulation are investigated and discussed, then the article will come to an end with the conclusion.

Simulation method

The method used in this study is the non-equilibrium Green's function (NEGF) whose efficiency has been proved for the simulation of different types of nanoscale devices including graphene nanoribbons and carbon nanotubes [20, 21]. The above-mentioned method properly models quantum behaviors; also, by providing an appropriate model, we can model the contact effects considering the nanoribbon atomic model [22]. In this method, the Poisson and the Schrödinger equations are solved in a self-consistent (SC) manner and after convergence and error reduction, the current is calculated using transport equation. The electron–phonon interaction enters Green's function as a scattering self-energy matrix (Σ_{SCAT}) and the phonon effects are regarded in the software simulation [22]. Green's function of the structure can be calculated using the following formula:

$$G(E) = [EI - H - \Sigma(E)]^{-1}, \quad (1)$$

where H is the Hamiltonian matrix of an armchair GNR, E

is the energy and $\Sigma(E)$ is the self-energy which has an extra term, $\Sigma_{\text{SCAT}}(E)$, compared to the ballistic mode.

$$\Sigma(E) = \Sigma_S(E) + \Sigma_D(E) + \Sigma_{\text{SCAT}}(E) \quad (2)$$

$\Sigma_S(E)$ and $\Sigma_D(E)$ are related to the self-energies of the source and drain, respectively, and $\Sigma_{\text{SCAT}}(E)$ is the electron–phonon scattering self-energy indicating the electron–phonon interaction.

The density of electrons and holes at different energies is calculated using correlation function (G) according to the following equation [23]:

$$G^n(E) = G \Sigma^{\text{in}} G^\dagger, \quad (3a)$$

$$G^p(E) = G \Sigma^{\text{out}} G^\dagger, \quad (3b)$$

where Σ^{in} and Σ^{out} , respectively, show the input and output scatterings, in which all the three terms of the electron–phonon scattering, drain, and source self-energy matrices participate:

$$\Sigma^{\text{in}} = \Sigma_D^{\text{in}} + \Sigma_S^{\text{in}} + \Sigma_{\text{SCAT}}^{\text{in}}, \quad (4a)$$

$$\Sigma^{\text{out}} = \Sigma_D^{\text{out}} + \Sigma_S^{\text{out}} + \Sigma_{\text{SCAT}}^{\text{out}}. \quad (4b)$$

Density of electrons and holes at point Z_j of the channel is obtained using the diagonal elements of the correlation matrix according to the following equation [24]:

$$n(z_j) = \frac{2}{3\pi a_{cc}} \int_{-\infty}^{+\infty} G_{j,j}^n(E) dE, \quad (5a)$$

$$p(z_j) = \frac{2}{3\pi a_{cc}} \int_{-\infty}^{+\infty} G_{j,j}^p(E) dE. \quad (5b)$$

Finally, the current equation in this model is calculated as follows [24]:

$$I_{\text{DS}} = \frac{ie}{\hbar\pi} \int_{-\infty}^{+\infty} b_{2q} (G_{1,2}^n - G_{2,1}^n) dE. \quad (6)$$

In the above equation, $b_{2q} = 2t \cos(\pi q/n)$ and $t \cong 3 \text{ eV}$ are the hopping parameter between two closer and further nearest neighbor A-GNR rings, respectively.

In graphene nanoribbons, the optical and acoustic phonon scatterings are among the dominant scattering mechanisms. Acoustic and optical phonon scatterings are elastic and non-elastic scattering events, respectively. To apply these effects to the electron–phonon scattering matrix, the Born approximation is used [23]. According to this approximation, in–out phonon scattering matrices are calculated using the following equations [25]:

$$\sum_{\text{SCAT}}^{\text{in}} = D_{\text{AP}} \times G^n(E) + D_{\text{OP}}(n_{\omega} + 1)G^n(E + h\omega_{\text{op}}) + D_{\text{OP}}(n_{\omega})G^n(E - h\omega_{\text{op}}), \tag{7a}$$

$$\sum_{\text{SCAT}}^{\text{out}} = D_{\text{AP}} \times G^p(E) + D_{\text{OP}}(n_{\omega} + 1)G^p(E - h\omega_{\text{op}}) + D_{\text{OP}}(n_{\omega})G^p(E + h\omega_{\text{op}}), \tag{7b}$$

where D_{ω} is the electron–phonon coupling parameter, n_{ω} is the phonon population or number of phonons at thermal equilibrium, and $G^{n(p)}$ is the electron’s correlation function (hole). $G^{n(p)}$ indicates the density of electrons (holes) at different energies, and D_{AP} and D_{OP} are calculated from the Hamiltonian matrix of the electron–phonon interaction according to what has been described. In this research, phonon energy is $h\omega_{\text{op}} = 196$ meV, electron–phonon coupling parameter is $D_{\text{AP}} = 0.01$ eV² and $D_{\text{OP}} = 0.07$ eV², and n_{ω} is calculated using the Bose–Einstein approximation according to the following equation [25, 26]:

$$n_{\omega} = \left(\exp\left(\frac{h\omega}{k_B T}\right) - 1 \right)^{-1}. \tag{8}$$

In Eqs. (7a) and (7b), the first term is related to acoustic phonon scattering. The mechanism of acoustic phonon scattering depends on the density of carriers at the same energy state. The second and third terms in the above equations are related to the optical phonon scattering, which shows phonon absorption and phonon emission processes, respectively. These instances are obvious in Fig. 1. Figure 1a, b is related to $\sum_{\text{SCAT}}^{\text{in}}$ and $\sum_{\text{SCAT}}^{\text{out}}$, respectively. In Fig. 1a, the electrons in higher energy states, $(E + h\omega_{\text{op}})$, lose energy via phonon emission and enter the energy state E . Also, the electrons with lower energy state, $(E - h\omega_{\text{op}})$, can enter the energy state E via phonon absorption. Therefore, the optical phonon scattering mechanism depends on the density of carriers not only in the same state, but also in higher and lower energy states. Further, for the carriers that exit an energy state

(Fig. 1b), like the previous state, we can assume two scenarios so that they can either exit from their energy state and go to higher energy states by phonon absorption or exit their energy state and go to lower energy states via phonon emission and getting cold.

Another notable point is that, regarding the voltage range within which we are working, it is necessary to assume up to 2 sub-bands for the calculation of the current in the used nanoribbon which is of armchair type with $N = 16$, because considering the distance between the sub-bands, the second sub-band practically plays an important role in the current calculation. Thus, besides considering intraband scattering effects, interband scattering effects must be also taken into account. These points are shown in Fig. 2.

Simulation results and discussion

In this section, the MOS-like GNR field-effect transistor is studied in the non-ballistic or dissipative conditions and the optical and acoustic phonon scattering effects are analyzed.

The simulated structure is shown in Fig. 3. The used nanoribbon is of armchair type with $N = 16$. The channel is an intrinsic one with the length of 15 nm and the source and drain are also 15 nm with the doping concentration of $N_{\text{sd}} = 10^{-2}$ dopant per atom. Oxide is of HfO₂ type with dielectric constant of $k = 16$ and its thickness is assumed to be 1.5 nm.

The $I_{\text{DS}}-V_{\text{DS}}$ characteristic curve of the above structure for the gate–source voltages as 0.4, 0.5, and 0.6 V is shown in Fig. 4. The simulations are performed in three situations: the ballistic transport, dissipative transport with only the acoustic phonon scattering, and finally dissipative transport with considering both optical and acoustic phonon scattering.

The results show that, due to causing back-scattering of the carriers toward the source and preventing them from

Fig. 1 The in-scattering and out-scattering process. **a** In-scattering, **b** out-scattering

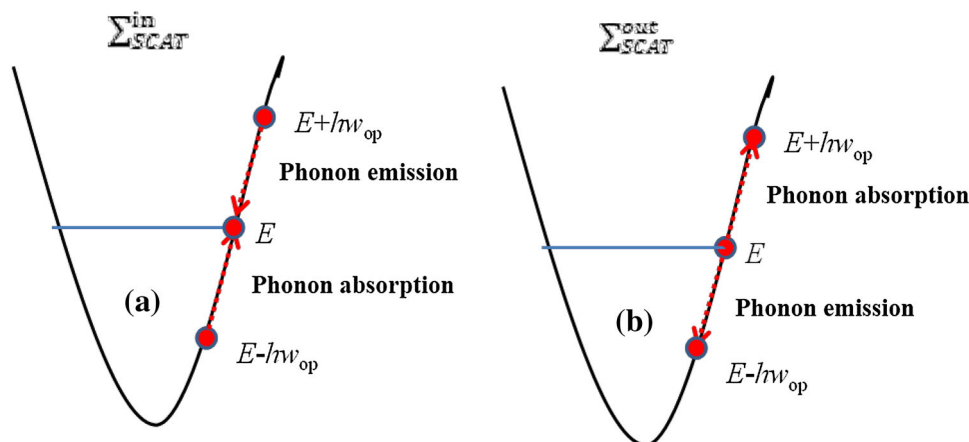


Fig. 2 The intraband and interband scattering process. **a** Intraband scattering, **b** interband scattering. Dashed and solid arrows related to elastic and inelastic scattering, respectively

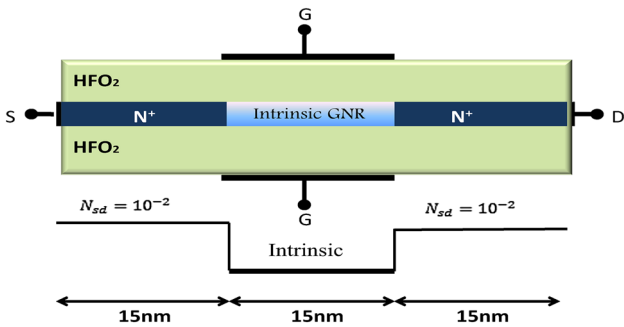
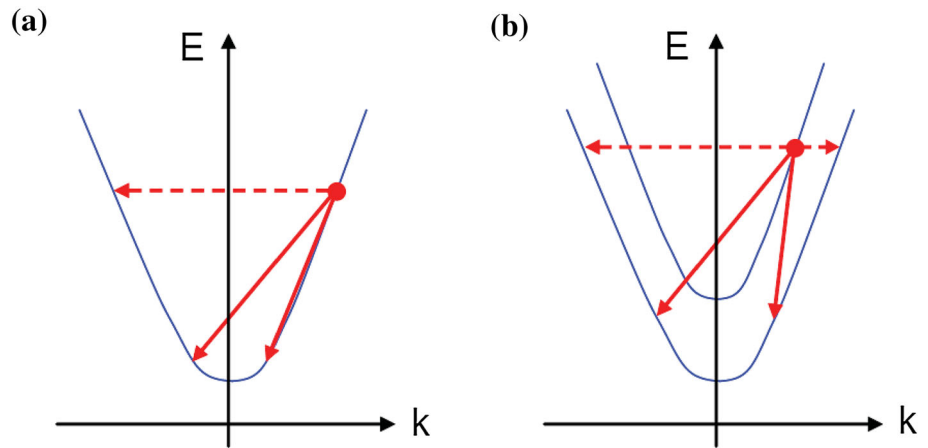


Fig. 3 The cross-sectional and doping profile of MOS-like GNR-FET. An HfO₂ dielectric layer with $\epsilon_{ox} = 16$ and $t_{ox} = 1.5$ nm is used. The source (drain) region is doped with 10^{-2} (dopant/atom) P (n) type impurities

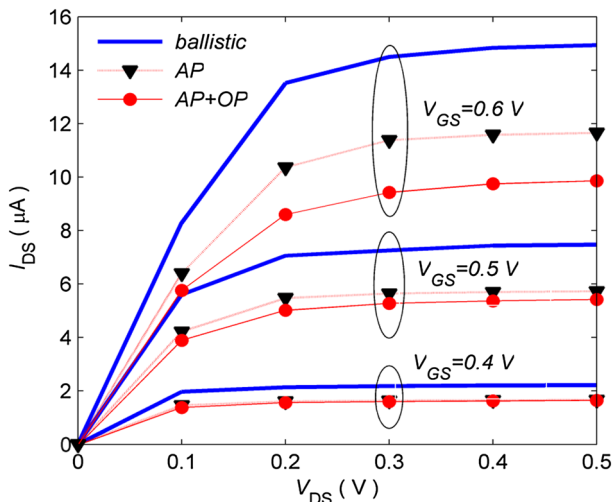


Fig. 4 Comparison of I_{DS} – V_{DS} characteristics of MOS-like GNR-FET for various $V_{GS} = 0.4, 0.5$ and 0.6 V. Lines, lines with triangles and lines with circles are for ballistic transport, with acoustic phonon scattering and with both acoustic and optical phonon scattering, respectively

reaching the drain, the ON current reduces by the phonon scatterings. The dominant scattering mechanism in a normal voltage range is the acoustic phonon scattering. As seen in the figure, the efficacy of the optical phonon scatterings is insignificant at low gate voltage compared to those of the acoustic ones. At the high gate voltage, the participation of the optical phonon scattering is considerable, the reason of which will be explained below. For example, at the gate voltage of 0.6 V, the current difference in the ballistic and dissipative mode is considerable, which could be related to the increased impact of optical phonon scatterings in the structure. The dependence of phonon scattering participation on the bias voltage can be better understood by drawing the energy-resolved current spectrum diagram. Figure 5 shows the energy-resolved current spectrum at the gate-source voltages of $0.4, 0.5$, and 0.6 V in the ballistic (a, b, and c) and non-ballistic (d, e, and f) modes. At low voltages (e.g., 0.4 V), the current density distribution window at the top of the conduction band in the channel region is lower than the optical phonon energy; therefore, the optical phonon scattering is almost stopped at the low voltage. With increasing the gate-source voltage (e.g., 0.6 V), the width of the window increases and the optical phonon scattering occurs. In this case, the back-going empty states will be filled by the scattered carriers and as a result the transistor current decreases.

The phonon scattering effects on the drain side can be seen in Fig. 5. The optical phonon scattering in the drain has less impact on the current, which can be explained as follows: on the drain side, the probability for the scattered carriers to reach the source is very low, because there is not enough energy to overcome the potential barrier at the drain-channel interface.

Then, the curve of current density in terms of energy for 0.6 V gate–source and 0.3 V drain–source voltage in the middle of the channel, i.e., at point $X = 22.5$ nm, is shown in Fig. 6. According to the figure, within the energy range of -0.2 eV $\leq E \leq 0.2$ eV, the current density is decreased

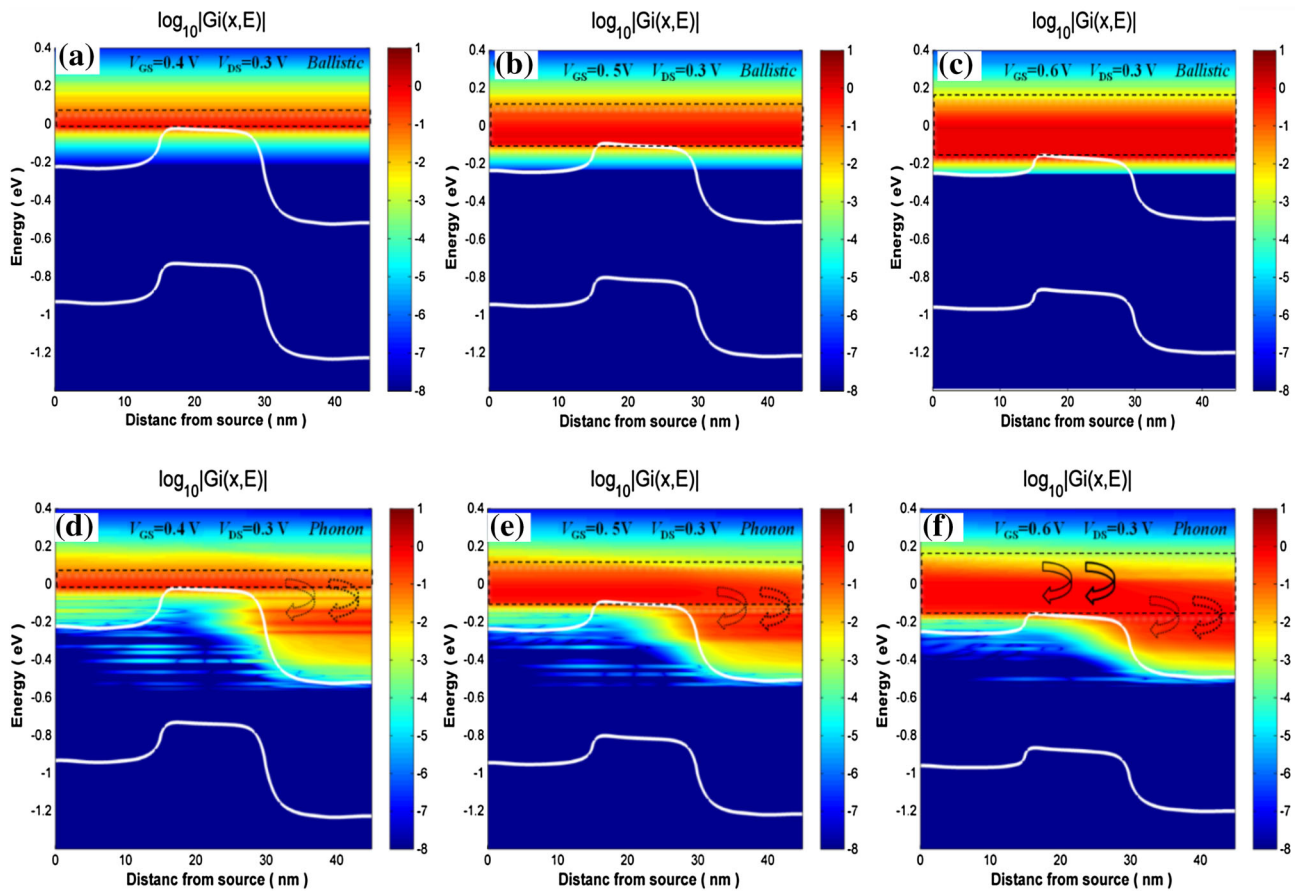


Fig. 5 Comparison of the energy band diagram (*white lines*) and the current spectrum (*color bar*) of the MOS-like GNR-FET for the ballistic transport at $V_{DS} = 0.3$ V and **a** $V_{GS} = 0.4$ V, **b** $V_{GS} = 0.5$ V

and **c** $V_{GS} = 0.6$ V and in the presence of phonon scattering (both AP and OP are treated) at **d** $V_{GS} = 0.4$ V, **e** $V_{GS} = 0.5$ V and **f** $V_{GS} = 0.6$ V, respectively

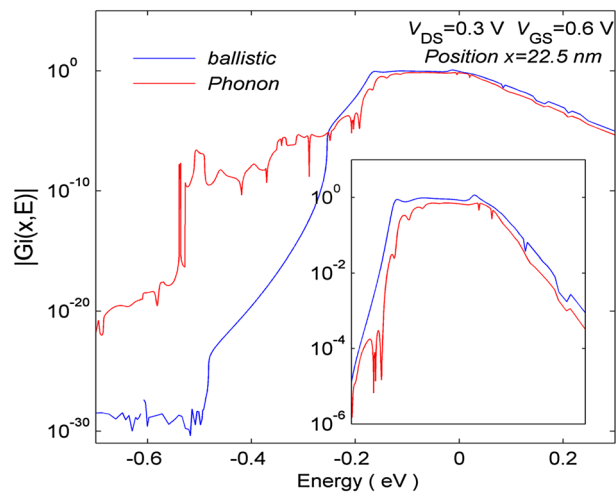


Fig. 6 Current density versus energy resolved of the MOS-like GNR-FET in the middle of the channel ($X = 22.5$ nm) at $V_{DS} = 0.3$ V and $V_{GS} = 0.6$ V under ballistic and dissipative transport. The *inset* shows current density within the energy range of $-0.2 \leq E \leq 0.2$ eV

in the non-ballistic mode compared to the ballistic one, which shows the accuracy of the explanations provided for the current reduction.

Moreover, in Fig. 7, the density of electrons at different energies along the transistor at $V_{DS} = 0.3$ V and gate-source voltages equal to 0.4, 0.5, and 0.6 V are presented considering the phonon effects (d, e, and g) and in the ballistic mode (a, b, and c). In the dissipative mode, the density of the electrons inside the energy-gap that is approximately one phonon energy less than the band-edge is considerable. These states are called quasi-continuous virtual states which are caused by the phonon scatterings [18, 19].

The $I_{DS}-V_{GS}$ diagram at $V_{DS} = 0.3$ V is demonstrated in Fig. 8. Continuous and dashed lines are related to the ballistic and dissipative modes, respectively. The phonon scattering causes an increase in the off-current, which is quite evident in this figure. In order to justify this behavior, the density of electrons at different energies in the ballistic and dissipative mode at $V_{DS} = 0.3$ V and $V_{GS} = -0.2$ V is

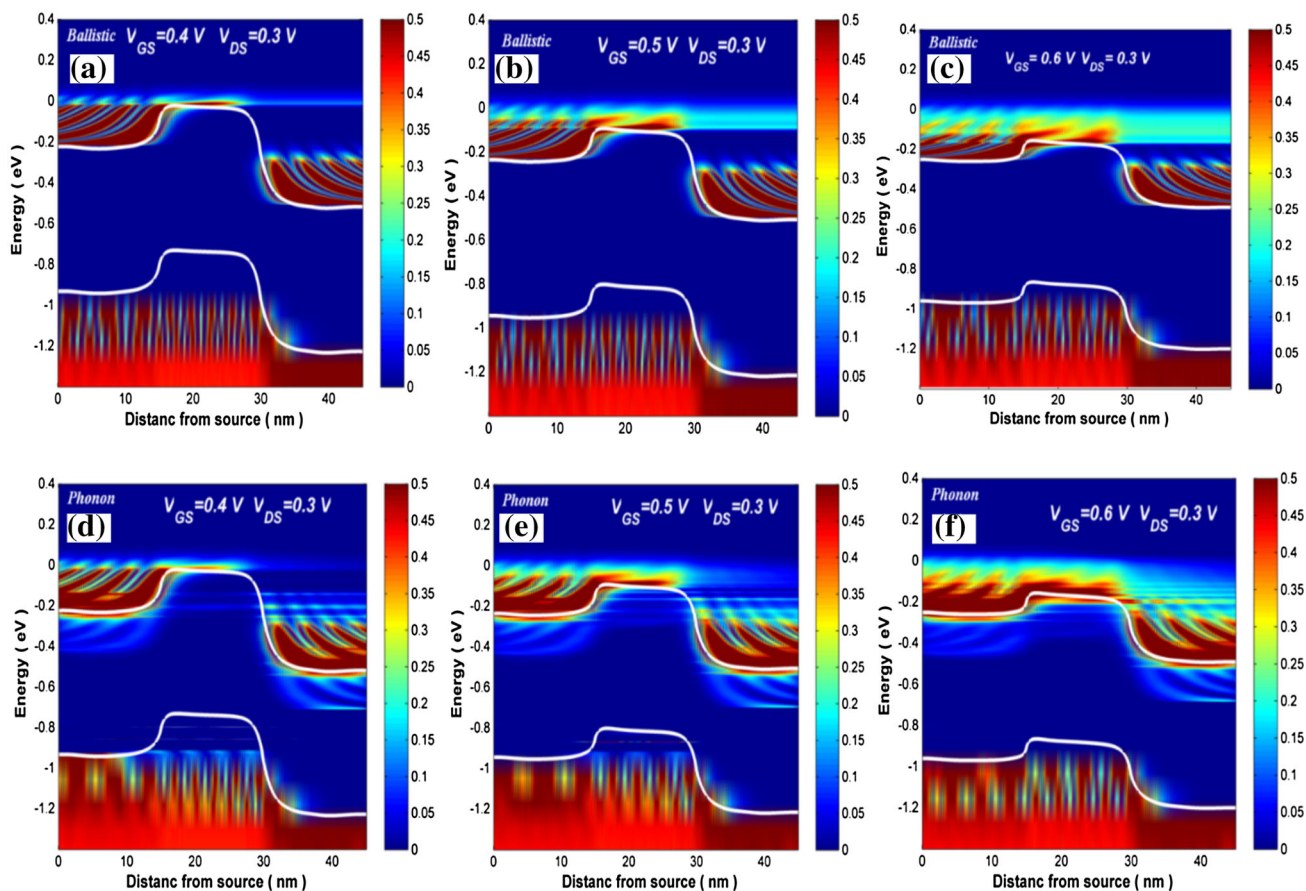


Fig. 7 Comparison of the energy band diagram (*white lines*) and the number of electrons per unit energy (*color bar*) of the MOS-like GNR-FET for the ballistic transport at $V_{DS} = 0.3$ V and

a $V_{GS} = 0.4$ V, **b** $V_{GS} = 0.5$ V and **c** $V_{GS} = 0.6$ V and in the presence of phonon scattering (both AP and OP are treated) at **d** $V_{GS} = 0.4$ V, **e** $V_{GS} = 0.5$ V and **f** $V_{GS} = 0.6$ V, respectively

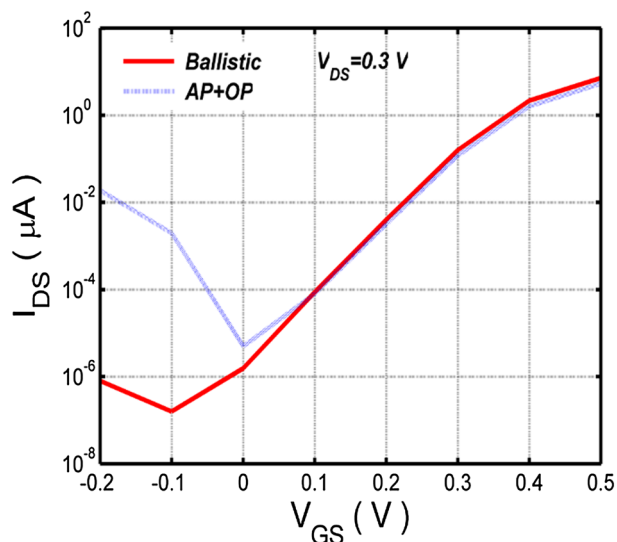


Fig. 8 I_{DS} - V_{GS} characteristics of the MOS-like GNR-FET at $V_{DS} = 0.3$ V for the ballistic transport and in the presence of both optical and acoustic phonon scattering

shown in Fig. 9a, b, respectively. As can be observed, in the presence of the acoustic and optical phonon scatterings, the density of the carriers at the valence band of the channel is increased compared with that of the ballistic mode, which could be attributed to the electrons located in the quasi-continuous virtual states that participate in the tunneling phenomenon. As explained, due to the phonon scattering, inside the energy-gap and approximately one phonon energy lower than the band-edge, a series of energy states are generated and the electrons can remain in these states for enough time to tunnel.

Then, the current density distribution at different energies for the mentioned MOSFET structure by considering both acoustic and optical phonon scattering at $V_{DS} = 0.3$ V and $V_{GS} = -0.2$ V is shown in Fig. 10. This figure represents that the current density distribution at different energies from the source to drain is shifted toward low energies, which is due to the phonon emission. The continuous lines of current distribution are related to those electrons which tunnel without scattering and go toward the drain. Those current distribution lines which are

Fig. 9 The band structure (white lines) and the number of electrons per unit energy (color bar) along the MOS-like GNR-FET at $V_{GS} = -0.2$ V and $V_{DS} = 0.3$ V for **a** ballistic and **b** dissipative mode

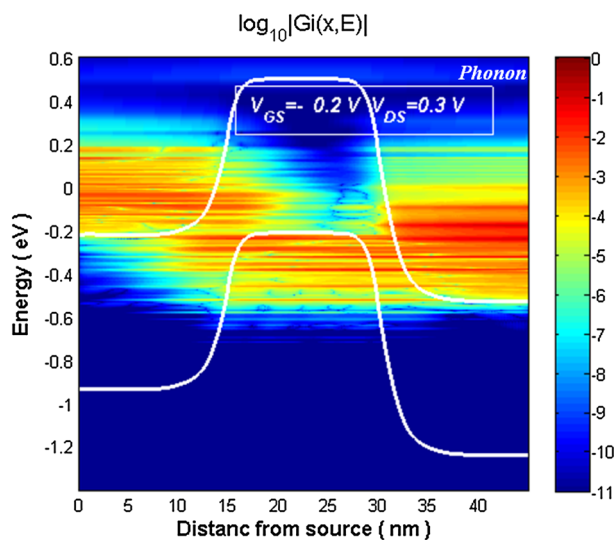
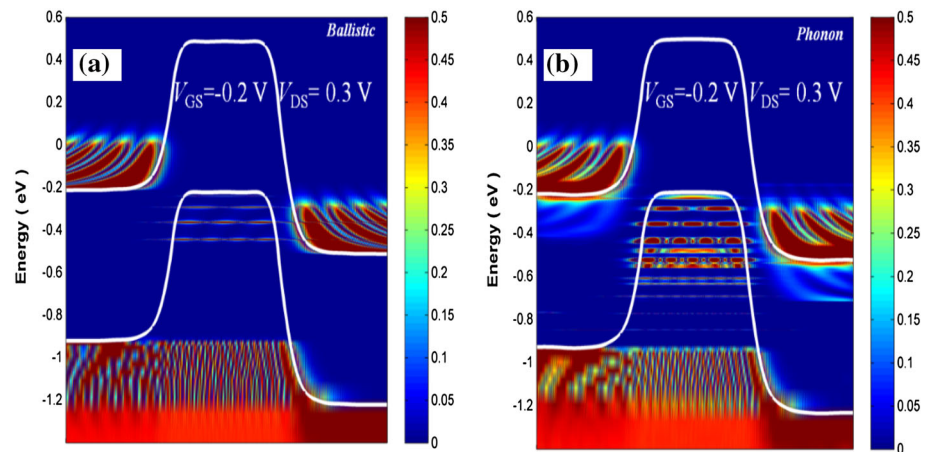


Fig. 10 Energy resolved current spectrum of the MOS-like GNR-FET at $V_{GS} = -0.2$ V and $V_{DS} = 0.3$ V

discontinued inside the channel depend on the electrons that can tunnel via phonon emission, and the lines starting within the energy gap are related to the electrons that first cause phonon emission and then tunnel toward the states with less energy.

Conclusion

The performances of MOS-like GNR field-effect transistor (GNRFET) have been extensively investigated in detail considering acoustic and optical phonon scattering. Quantum mechanical simulations based on a mode-space approach of the non-equilibrium Green's function formalism are used to extract characteristics of the devices. It has been shown that the operation of GNR-FET is mainly limited by the inclusion of electron–phonon interaction. Simulation results indicate that under on-state operation,

the impact of optical phonon scattering on the current degradation becomes noticeable at large gate biases. Also band-to-band tunneling regime is dominated by the phonon-assisted tunneling and sub-threshold swing and off-current are deteriorated by this phenomenon.

Open Access This article is distributed under the terms of the Creative Commons Attribution 4.0 International License (<http://creativecommons.org/licenses/by/4.0/>), which permits unrestricted use, distribution, and reproduction in any medium, provided you give appropriate credit to the original author(s) and the source, provide a link to the Creative Commons license, and indicate if changes were made.

References

- Chen, Y.-Y., Sangai, A., Gholipour, M., Chen, D.: Graphene nano-ribbon field-effect transistors as future low-power devices. In: Int. Symp. Low Power Electron. Des., IEEE, pp. 151–156 (2013). doi:[10.1109/ISLPED.2013.6629286](https://doi.org/10.1109/ISLPED.2013.6629286)
- Xie, Q., Lee, C.J., Xu, J., Wann, C., Sun, J.Y.C., Taur, Y.: Comprehensive analysis of short-channel effects in ultrathin SOI MOSFETs. IEEE Trans. Electron Devices **60**, 1814–1819 (2013). doi:[10.1109/TED.2013.2255878](https://doi.org/10.1109/TED.2013.2255878)
- Fitzgerald, B.M.: Transistors: types, materials and applications. Nova Science Publisher, Hauppauge (2010)
- Chen, E.P.D., Chilstedt, S., Dong, C.: What everyone needs to know about carbon-based nanocircuits. In: Des. Autom. Conf. (2010)
- Sanaeepur, M., Goharrizi, A.Y., Sharifi, M.J.: Performance analysis of graphene nanoribbon field effect transistors in the presence of surface roughness. IEEE Trans. Electron Devices **61**, 1193–1198 (2014). doi:[10.1109/Ted.2013.2290049](https://doi.org/10.1109/Ted.2013.2290049)
- Chen, Z., Lin, Y.-M., Rooks, M.J., Avouris, P.: Graphene nano-ribbon electronics. Phys. E Low Dimens. Syst. Nanostruct. **40**, 228–232 (2007). doi:[10.1016/j.physe.2007.06.020](https://doi.org/10.1016/j.physe.2007.06.020)
- Yousefi, R., Saghafi, K., Moravvej-Farshi, M.K.: Numerical study of lightly doped drain and source carbon nanotube field effect transistors. IEEE Trans. Electron Devices **57**, 765–771 (2010). doi:[10.1109/TED.2010.2041282](https://doi.org/10.1109/TED.2010.2041282)
- Ghoreishi, S.S., Saghafi, K., Yousefi, R., Moravvej-Farshi, M.K.: Graphene nanoribbon tunnel field effect transistor with lightly doped drain: numerical simulations. Superlattices Microstruct. **75**, 245–256 (2014). doi:[10.1016/j.spmi.2014.07.042](https://doi.org/10.1016/j.spmi.2014.07.042)



9. Naderi, A.: Theoretical analysis of a novel dual gate metal-graphene nanoribbon field effect transistor. *Mater. Sci. Semicond. Process.* **31**, 223–228 (2015). doi:[10.1016/j.mssp.2014.11.051](https://doi.org/10.1016/j.mssp.2014.11.051)
10. Ghoreishi, S.S., Saghafi, K., Moravvej-Farshi, M.K.: A novel graphene nano-ribbon field effect transistor with Schottky tunneling drain and Ohmic tunneling source. *Mod. Phys. Lett. B* **27**, 1350189 (2013). doi:[10.1142/S0217984913501893](https://doi.org/10.1142/S0217984913501893)
11. Yoon, Y., Ouyang, Y., Cuo, J.: Scaling behaviors of graphene nanoribbon FETs. In: 65th DRC Device Res. Conf., pp. 271–272 (2007). doi:[10.1109/DRC.2007.4373750](https://doi.org/10.1109/DRC.2007.4373750)
12. Fiori, G., Iannaccone, G.: Simulation of graphene nanoribbon field effect transistors. *IEEE Electron Devices Lett.* **28**, 760–762 (2007). doi:[10.1109/LED.2007.901680](https://doi.org/10.1109/LED.2007.901680)
13. Liang, G., Neophytou, N., Nikonov, D.E., Lundstrom, M.S.: Performance projections for ballistic graphene nanoribbon field-effect transistors. *IEEE Trans. Electron Devices* **54**, 677–682 (2007). doi:[10.1109/TED.2007.891872](https://doi.org/10.1109/TED.2007.891872)
14. M. A., F. M., Jalili, S.: Low-field phonon limited mobility in graphene nanoribbon. In: 4th Int. Conf. Nanostructures, Kish Island, Iran, pp. 12–14 (2012)
15. Akhavan, N.D., Jolley, G., Umana-Membreno, G.A., Antoszewski, J., Faraone, L.: Phonon limited transport in graphene nanoribbon field effect transistors using full three dimensional quantum mechanical simulation. *J. Appl. Phys.* (2012). doi:[10.1063/1.4764318](https://doi.org/10.1063/1.4764318)
16. Koswatta, S.O., Lundstrom, M.S., Nikonov, D.E.: Influence of phonon scattering on the performance of *p-i-n* band-to-band tunneling transistors. *Appl. Phys. Lett.* (2008). doi:[10.1063/1.2839375](https://doi.org/10.1063/1.2839375)
17. Koswatta, S.O., Lundstrom, M.S., Nikonov, D.E.: Performance comparison between *p-i-n* tunneling transistors and conventional MOSFETs. *IEEE Trans. Electron Devices* **56**, 456–465 (2009). doi:[10.1109/TED.2008.2011934](https://doi.org/10.1109/TED.2008.2011934)
18. Koswatta, S.O., Lundstrom, M.S., Anantram, M.P., Nikonov, D.E.: Simulation of phonon-assisted band-to-band tunneling in carbon nanotube field-effect transistors. *Appl. Phys. Lett.* **87**, 1–3 (2005). doi:[10.1063/1.2146065](https://doi.org/10.1063/1.2146065)
19. Koswatta, S.O., Lundstrom, M.S., Nikonov, D.E.: Band-to-band tunneling in a carbon nanotube metal-oxide-semiconductor field-effect transistor is dominated by phonon-assisted tunneling. *Nano Lett.* **7**, 1160–1164 (2007). doi:[10.1021/nl062843f](https://doi.org/10.1021/nl062843f)
20. Datta, S.: Nanoscale device modeling: the Green's function method. *Superlattices Microstruct.* **28**, 253–278 (2000). doi:[10.1006/spmi.2000.0920](https://doi.org/10.1006/spmi.2000.0920)
21. Datta, S.: Quantum transport: atom to transistor. Cambridge University Press, England (2005). doi:[10.1017/CBO9781139164313](https://doi.org/10.1017/CBO9781139164313)
22. Guo, J.: Carbon nanotube electronics: modeling: physics and applications. Purdue University, West Lafayette (2004)
23. Guo, J.: A quantum-mechanical treatment of phonon scattering in carbon nanotube transistors. *J. Appl. Phys.* (2005). doi:[10.1063/1.2060942](https://doi.org/10.1063/1.2060942)
24. Koswatta, S.O., Hasan, S., Lundstrom, M.S.: Non-equilibrium Green's function treatment of phonon scattering in carbon nanotube transistors (n.d.)
25. Hasan, S.: Electron phonon interaction in carbon nanotube devices. Purdue University, West Lafayette, Indiana (2007)
26. Nikonov, G.B.D., Pal, H.: Scattering in NEGF: made simple. (2009). <http://nanohub.org/resources/7772>

